Electronic Supplementary Material (ESI) for Materials Horizons.

Supplementary information for

Interface limited hole extraction from methyl-ammonium lead iodide films

Oskar Blaszczyk, Lethy Krishnan Jagadamma, Arvydas Ruseckas, Muhammad T. Sajjad, Yiwei Zhang, Ifor D.W. Samuel

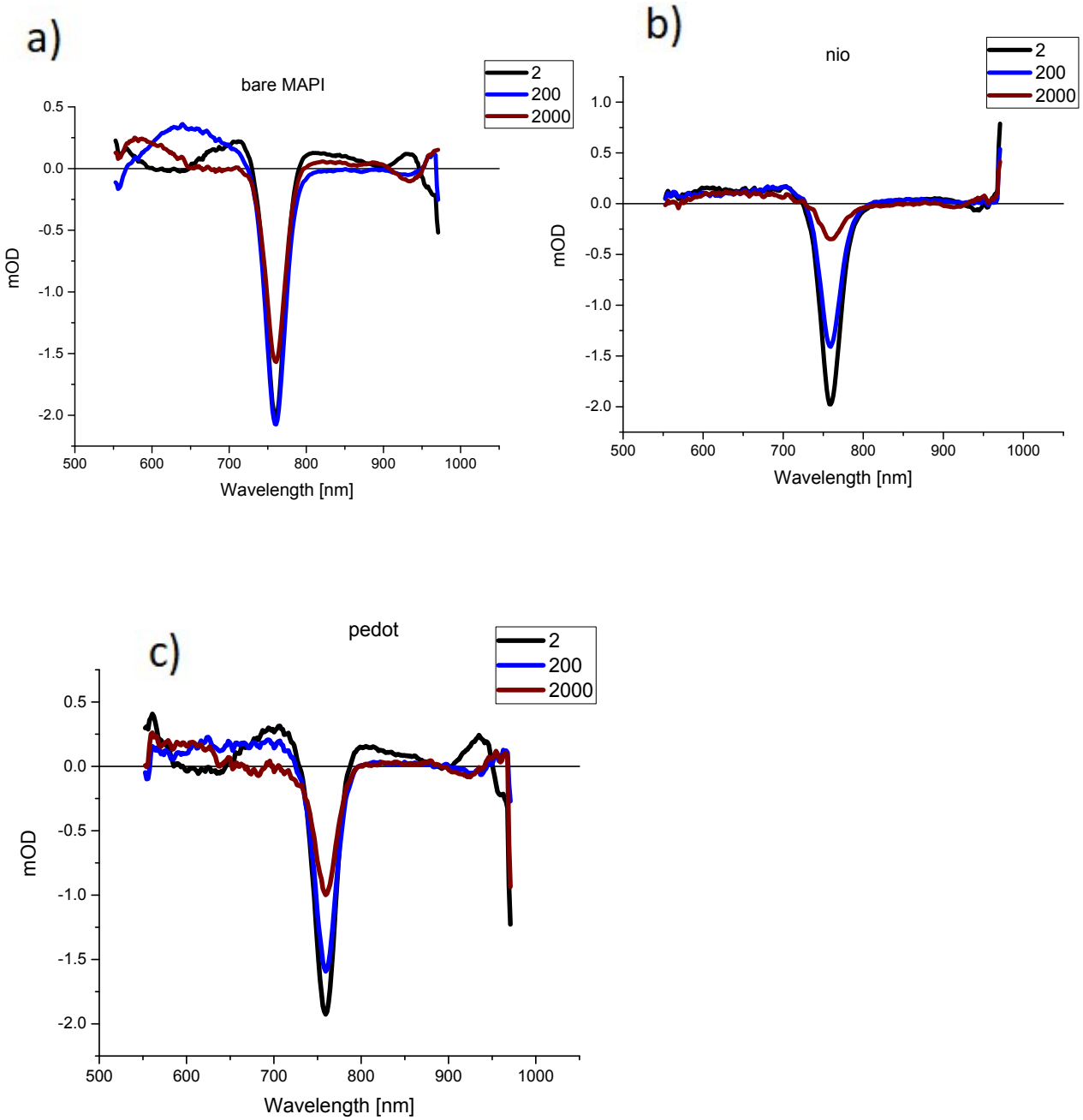

Figure S1. Transient absorption spectra of a) bare MAPI on glass, b) MAPI on NiO and c) MAPI on PEDOT:PSS shown for 2 ps, 200 ps and 2000 ps delay after the pump pulse.

The morphology of the perovskite grown on top of the NiO and PEDOT:PSS substrates was investigated using scanning electron microscopy (SEM) and the following images were acquired

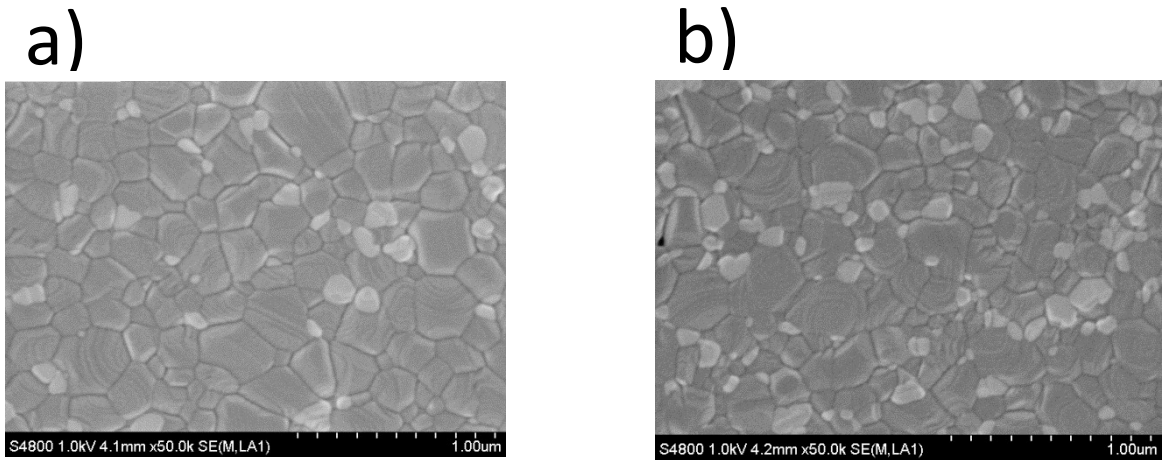

Fig. S2. The SEM images of the perovskite active layer grown on top of a) NiO and b)PEDOT:PSS

XRD measurements on MAPbI3/PEDOT:PSS and MAPbI3/NiO were performed to understand the crystalline properties of the perovskite layer.

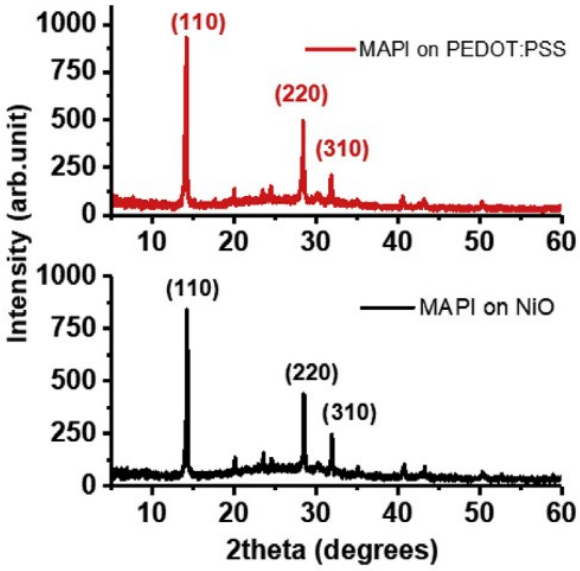

Figure S3. X-ray diffraction pattern for $CH_3NH_3PbI_3$ deposited on top of PEDOT:PSS and NiO. The data was collected by the authors in and included in a previous publication on a different topic[1].

Similar intensities of diffraction peaks at 14.1° and 28.5°, corresponding to the (110) and the (220) planes of the tetragonal phase, can be seen in figure S2. The similarities between the data for the perovskite layer grown on top of the different substrates suggest little difference in crystallinity between the samples. We therefore conclude that the defect states in the perovskite bulk should also be similar for both $CH_3NH_3PbI_3/PEDOT{:}PSS$ and $CH_3NH_3PbI_3/NiO$.

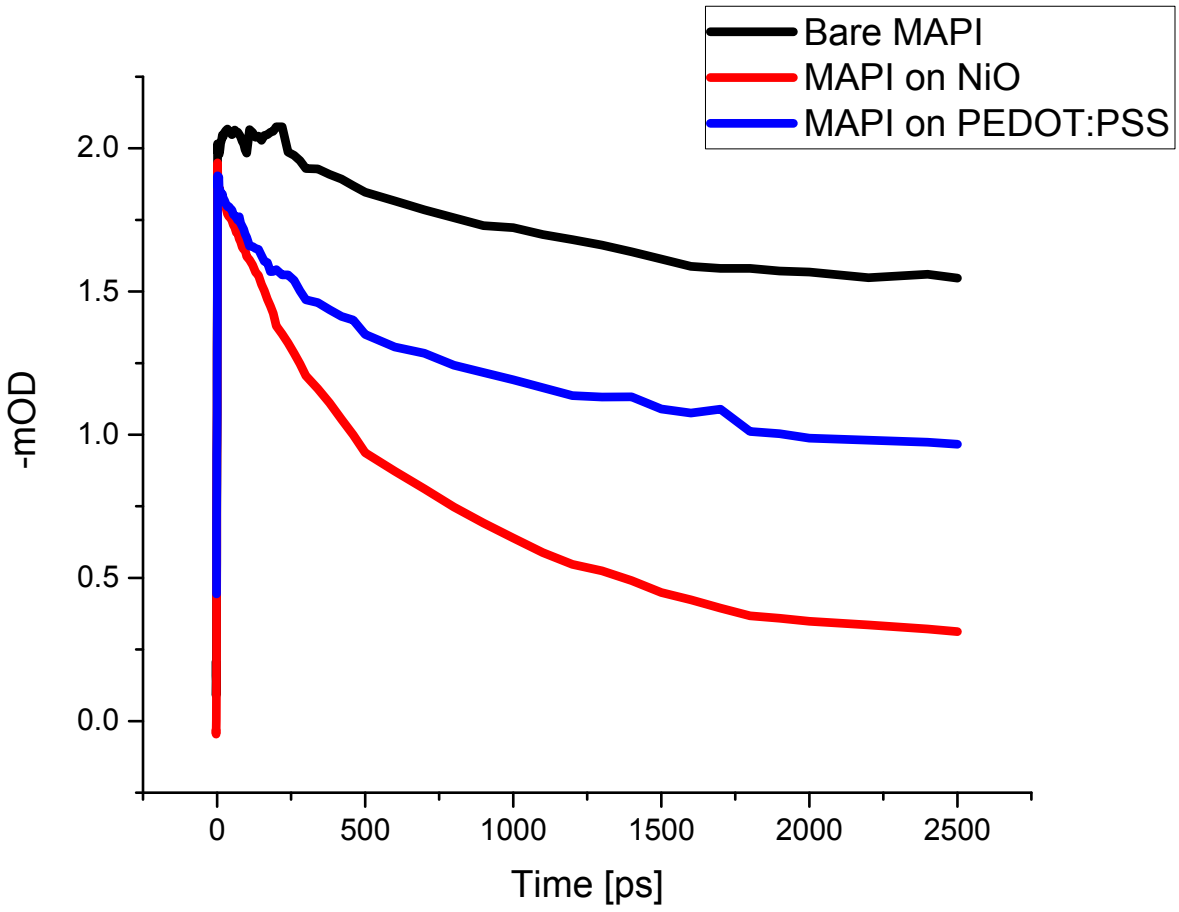

Figure S4. Decays of ground state bleaching at 760 nm for MAPI on glass(black line), MAPI on NiO (red line) and MAPI on PEDOT:PSS (blue line)

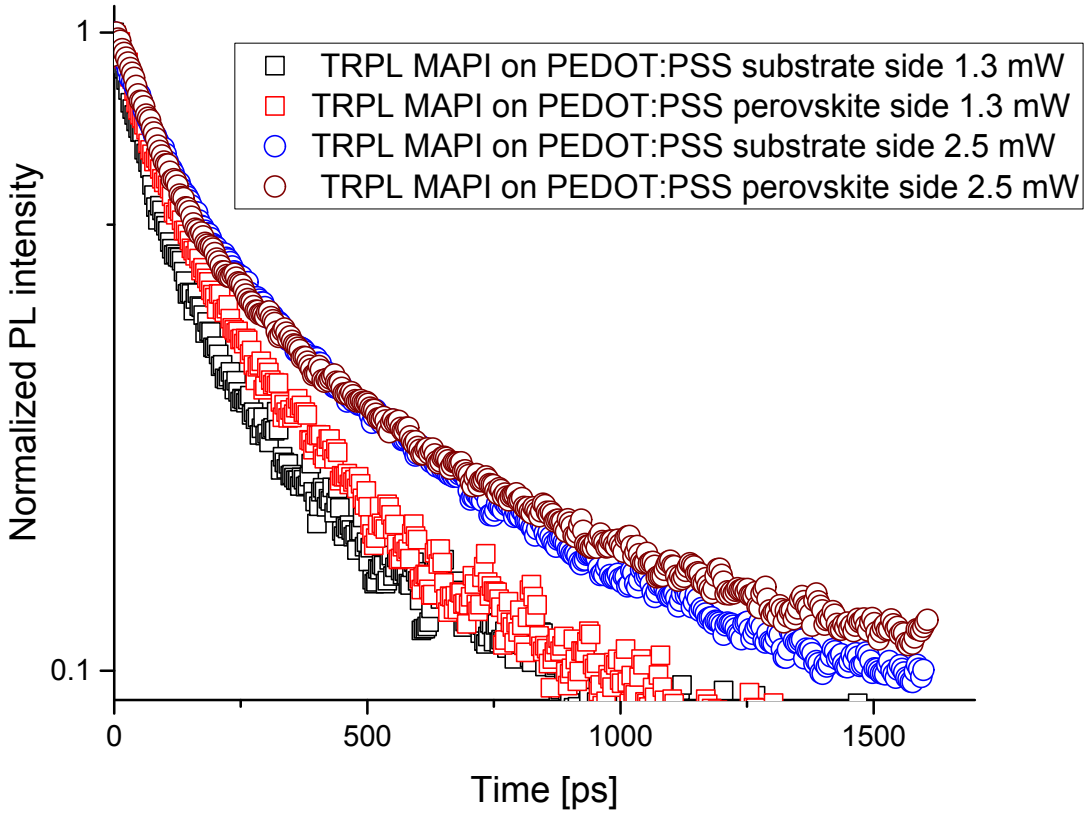

Figure S5. Excitation intensity dependence of PL decays of MAPI on PEDOT:PSS taken from two sides of the sample.

To determine the diffusion coefficient and the interfacial transfer rate (quenching velocity) the diffusion equation was solved numerically. This was done using the NDSolveValue function in Mathematica 11.0. The solution method was restricted to the" MethodOfLines". The solution to the equation yielded a spatio-temporal distribution of holes in the perovskite active layer and can be seen below for the case of $CH_3NH_3PbI_3/NiO$ with illumination from the perovskite side:

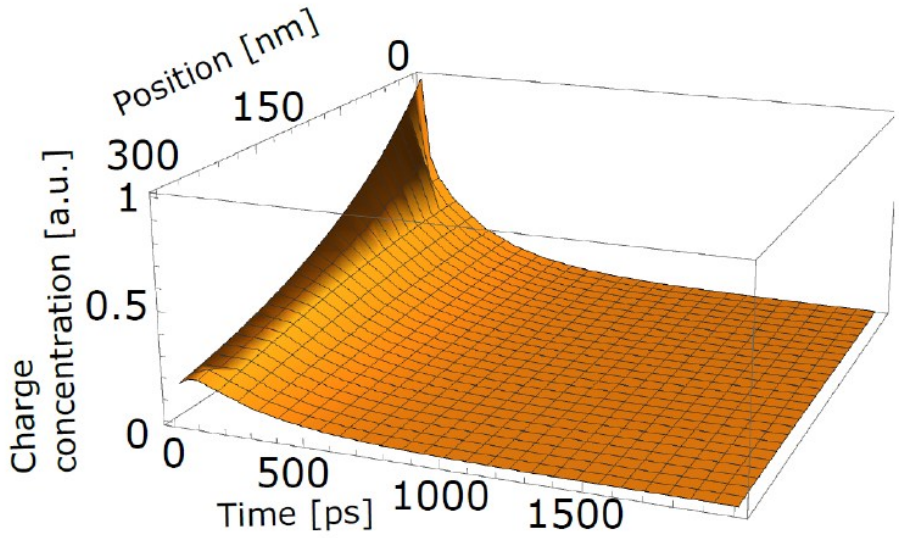

Figure S6. Normalized spatio-temporal distribution of charge carriers within the perovskite active layer for the imperfect quencher case, with illumination from the perovskite side and the NiO layer at position =300 nm.

The initial carrier distribution of was calculated from Beer-Lambert law. The 300 nm thick perovskite film showed absorbance of 0.7 at 640 nm excitation wavelength. The carrier recombination without the extraction layer was measured in $CH_3NH_3PbI_3$ thin film on glass and fitted with a two-exponential decay to account for $CH_3NH_3PbI_3/vacuum$ and bulk recombination. The following equation and values were fitted to the data : $A\,e^{-\frac{t}{\tau_1}} + B\,e^{-\frac{t}{\tau_2}}$ with A=0.63 and $\tau_1 = 10.5\,ns$ and B=0.37 and $\tau_2 = 0.6\,ns$ which are typical values for the natural decay in $CH_3NH_3PbI_3$ perovskite, relating to bulk and surface recombination respectively. The carrier recombination in the absence of the quencher layer was used in the solution of the diffusion equation to account for the decay pathways common to films with and without the quenching layer.

To highlight the importance of the illuminating from each side in the photoluminescence surface quenching experiment, a simulated time resolved PL decay is plotted in the graph below together with experimental data. The model assumes a perfect quencher (infinite quenching rate) at the interface with the hole extracting material. A large misfit can be seen for the case of illumination from the substrate (NiO) side where a pronounced dip develops in the model, due to very fast quenching of holes created near the interface. The value of the diffusion coefficient in the model is 1.06 cm^2/s.

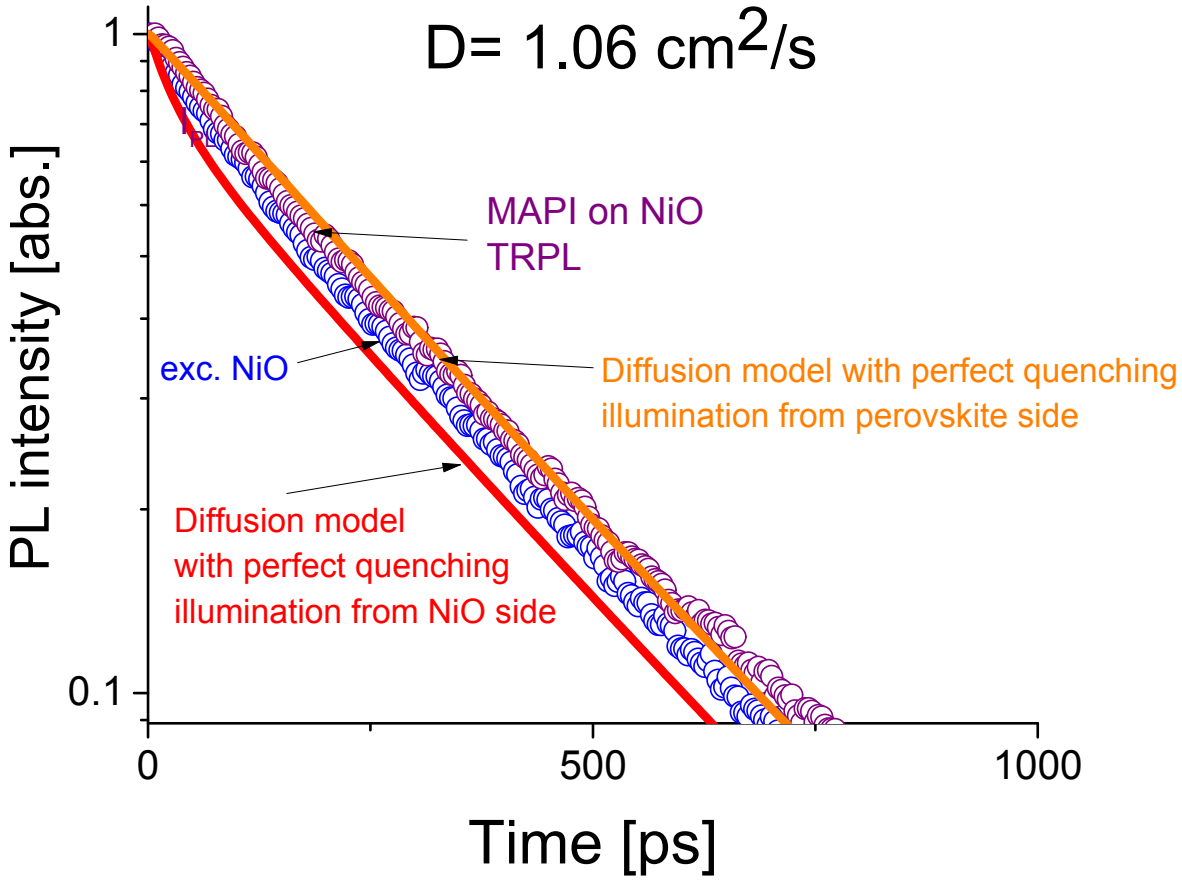

Figure S7. *Perfect quencher model fitted to PL decays for the case of perovskite side illumination (orange line) and substrate side illumination (red line). The misfit is produced only for the substrate side illumination, both fits assume instantaneous quenching and D=1.06 cm^2/s.*

PL surface quenching with illumination from each side was used to obtain PL decay data for MAPI on NiO. A range for the values of D has been identified by fitting the imperfect quencher model to the experimental data. This range is between

$$D = (1.8\frac{cm^2}{s} - 2.5\frac{cm^2}{s}) \pm 0.1\ cm^2/s$$

The corresponding range of quenching velocity is:

$$k = (3.4 \times 10^5 - 3.8 \times 10^5\frac{m}{s}) \pm 0.1 \times 10^5\frac{m}{s}$$

The plots of the fits for these values can be seen in the figure below.

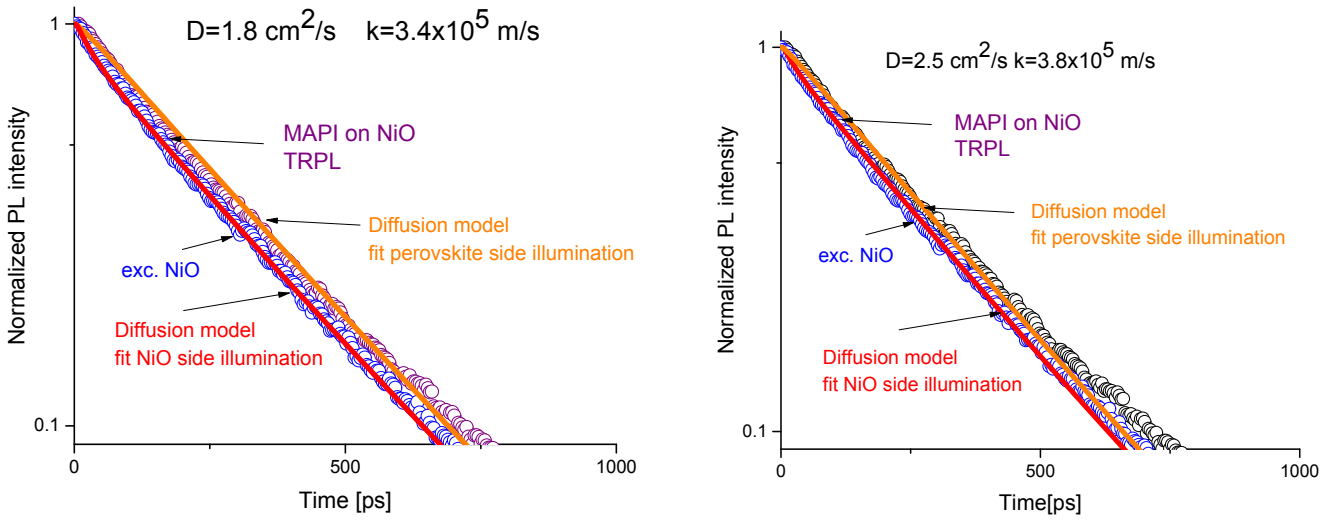

Figure S8. PL decays for MAPI on NiO taken from each side of the sample. The fits are done for two limiting values of D that produce acceptable fits, giving the range of values of D and k.

Increasing or decreasing the value of the diffusion coefficient past these values produces fits that do not overlap with the data sets sufficiently, as seen in the figure below. The D values showed here are D=1 cm^2/s. and D=4 cm^2/s.

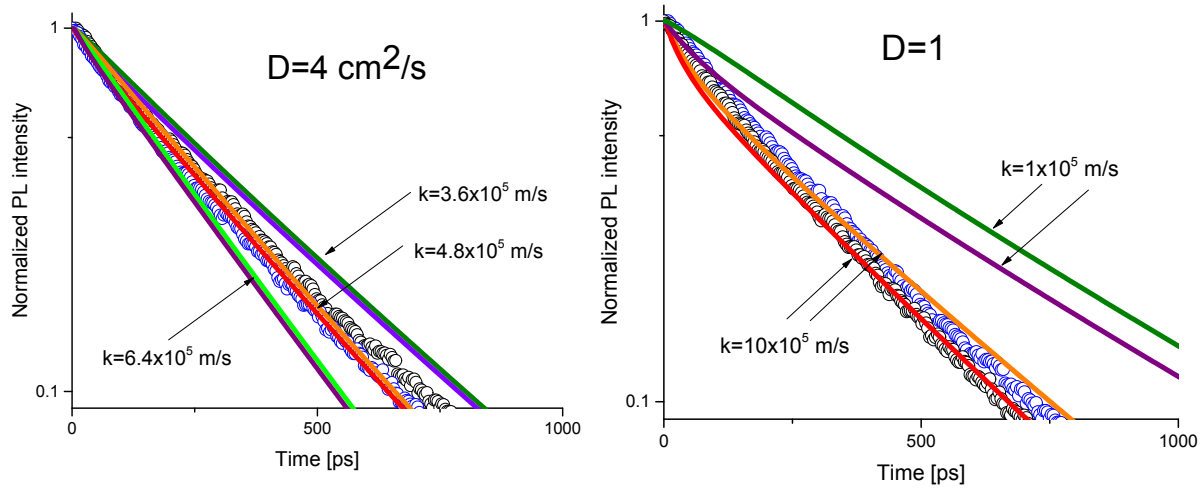

Figure S9. PL decays of MAPI on NiO illuminated from two sides. The solid lines show the simulated PL decays for different D and k values.

Large values of the diffusion coefficient tend to bring the two modelled PL decays close together. The relative importance of the interface decreases and holes decay similarly. The data show some separation so this high value of D cannot fit the data.

Small values of D lead to a separation of the two models that is too large to fit the data, in addition, the fast quenching case causes there a dip to develop at early times in one of the simulated PL decays. This occurs for the case of illumination from the substrate side, where most holes are created near the interface. This value of D, therefore, does not produce a satisfactory fit.

The fitting of the entire TRPL for the case of PEDOT:PSS hole extracting layer was not possible using a single quenching rate. This is due to the time varying quenching rate which suggests a time varying velocity across the interface. Instead, the TRPL was truncated into three parts and an average quenching rate for the selected time windows was fit. The results can be seen in the figure below.

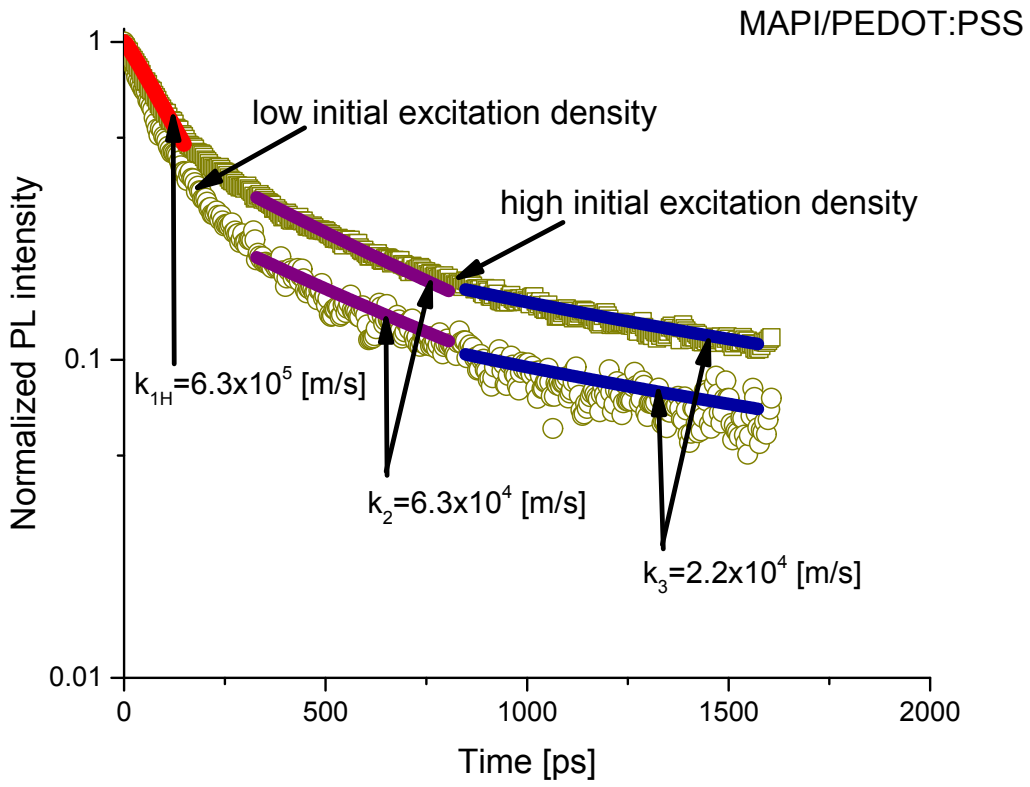

Figure S10. TRPL of $CH_3NH_3PbI_3/PEDOT{:}PSS$ *together with the global fit using the diffusion model from eq. number for a))* $1.3 \times 10^{16}\ cm^{-3}$ *average charge carrier density and b)* $2.7 \times 10^{16}\ cm^{-3}$

In the first 150 ps the TRPL decay proceeds at a similar rate for the case of both initial excitation densities. After the initial 150 ps there is a significant slowing down of the quenching rate for the sample with higher initial charge density while the lower initial charge does not show such a strong effect. After the initial 350 ps the TRPL decay data for both initial excitation densities becomes parallel (same gradient) suggesting the decay is taking place at the same, albeit slower, rate. This trend continues until the end of the time window of 1.5 ns.

The TRPL decay rate is determined by fitting to the experimental data using the imperfect quencher model with the same diffusion coefficient as for the case of NiO ($D = (2.2 \pm 0.4)\ cm^2/s$) and for the 0-150 ps time window it is $k_1 = (6.3 \pm 0.35) \times 10^5 \frac{m}{s}$, in the 350-810 ps time window the decay rate was determined to be $k_2 = (6.3 \pm 0.22) \times 10^4 \frac{m}{s}$ and for the 810-1500 ps time window the rate decreased even further to a value of $k_3 = (2.2 \pm 0.8) \times 10^4 \frac{m}{s}$.

Initially the quenching velocity in the $CH_3NH_3PbI_3/PEDOT{:}PSS$ films is faster than in the case of $CH_3NH_3PbI_3/NiO$ where the global quenching velocity has the value $k_1 = (3.6 \pm 0.2) \times 10^5 \frac{m}{s}$. This is consistent with another decay pathway being present at early times in the $CH_3NH_3PbI_3/PEDOT{:}PSS$ films compared with $CH_3NH_3PbI_3/NiO$ and can be explained by the presence of more surface traps at the $CH_3NH_3PbI_3/PEDOT{:}PSS$ interface than in the case of $CH_3NH_3PbI_3/NiO$. This is further supported by the earlier slowing down of the decay rate in the sample with higher initial charge density, consistent with a faster filling of traps. Beyond 350 ps the quenching velocity slows down significantly, to values an order of magnitude lower than in $CH_3NH_3PbI_3/NiO$. This is consistent with the accumulation of holes at the $CH_3NH_3PbI_3/PEDOT{:}PSS$ interface which would impede further transport across the interface.

Bibliography:

1. L. K. Jagadamma, O. Blaszczyk, M. T. Sajjad, A. Ruseckas and I. D. W. Samuel, *Sol. Energy Mater. Sol. Cells*, 2019, **201**, 110071.